Automated Detection of Lung Nodules with Three-dimensional Convolutional Neural Networks

Gustavo Pérez and Pablo Arbeláez

Universidad de los Andes, Cra 1 N 18A - 12, Bogotá, Colombia

ABSTRACT

Lung cancer is the cancer type with highest mortality rate worldwide. It has been shown that early detection with computer tomography (CT) scans can reduce deaths caused by this disease. Manual detection of cancer nodules is costly and time-consuming. We present a general framework for the detection of nodules in lung CT images. Our method consists of the pre-processing of a patient's CT with filtering and lung extraction from the entire volume using a previously calculated mask for each patient. From the extracted lungs, we perform a candidate generation stage using morphological operations, followed by the training of a three-dimensional convolutional neural network for feature representation and classification of extracted candidates for false positive reduction. We perform experiments on the publicly available LIDC-IDRI dataset. Our candidate extraction approach is effective to produce precise candidates with a recall of 99.6%. In addition, false positive reduction stage manages to successfully classify candidates and increases precision by a factor of 7.000.

Keywords: Lung cancer, lung nodules, deep learning, computer aided diagnosis

1. INTRODUCTION

Cancer is the main cause of death worldwide, accounting for 8.2 million deaths per year approximately. Lung cancer leads this list with 1.69 million deaths per year.[1] Early detection with the aid of CT scans has shown to reduce lung cancer mortality by 16% to 20%, compared to standard chest x-ray among adults.[2] In January 2013, the American Cancer Society issued guidelines for the early detection of lung cancer based on a systematic review of the evidence. These guidelines endorse a process of shared decision-making between clinicians who have access to high-volume lung cancer screening programs.[2] However, the consensus in lung-nodule detection by radiologists is less than 60% when detecting nodules of any size.[3] As shown in Figure 1, the difficulty in the early diagnosis of lung cancer is due to the variability in shape and size of nodules, and the high unbalance between the nodules and other lung structures and tissues.

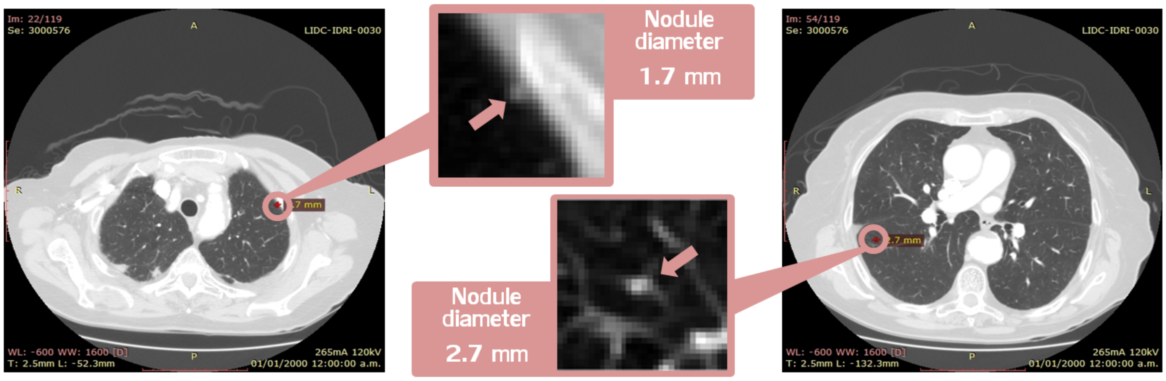

Figure 1. Examples of annotated nodules <3mm on the LIDC-IDRI dataset. **Left.** Juxtapleural nodule of diameter 1.7mm. **Right.** Parenchymal nodule of diameter 2.7mm surrounded by vessels.

Further author information:
Gustavo Pérez: E-mail: ga.perezs@uniandes.edu.co

A great amount of research has been conducted over the past two decades in computer-aided detection (CAD) systems for lung nodules in CT scans.[45] A large number of systems for nodule detection have been proposed in the literature.[6] However, low sensitivity and high false-positive rates are still issues that prevent these systems from being used in the daily clinical practice.

Recently, significant research has been done with the use of deep learning techniques, and its recent success for detection, segmentation, and recognition on natural and medical images like detection of skin cancer[7] makes inescapable the application of these machine learning methods for lung cancer CAD systems. Due to the variability and the high unbalance between the nodules and other lung structures, handcrafted feature extraction is a difficult task. Learned features from a convolutional neural network yield conceptual abstractions by each layer in a hierarchical way and outperform handcrafted features.

Our general framework is shown in Figure 2. To achieve the goal of nodule detection from a CT scan, we implement a stage for pre-processing using filtering, and the lungs extraction from the entire volume using a mask previously calculated for each patient. From the extracted lungs, we perform a candidate generation using morphological operations such as opening by reconstruction, the calculation of regional maxima, etc. We use the extracted candidates to train a three-dimensional convolutional neural network for nodule classification and false positive reduction. We conduct experiments on the currently largest publicly available database for nodule detection, the LIDC-IDRI.[3] We develop a computer-aided system for the detection of lung nodules that nearly reaches human performance.

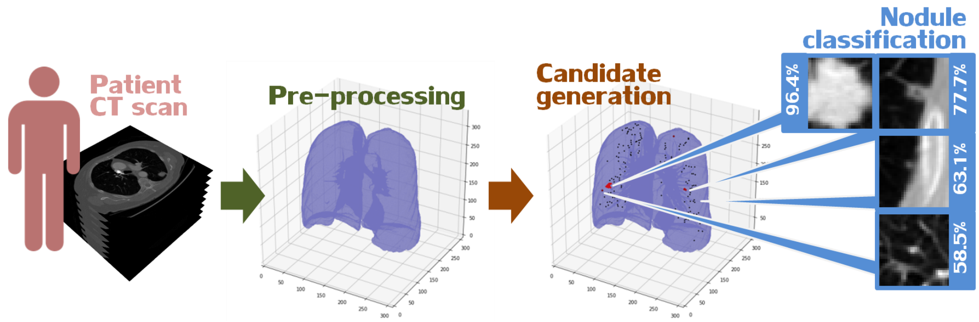

Figure 2. Proposed method: pre-processing for noise reduction and lung extraction with a mask, candidate generation with morphological operations, and nodule classification with a three-dimensional convolutional neural network to reduce false positives and increase precision.

2. RELATED WORK

Several algorithms rely on thresholding methods and morphological operations for nodule segmentation, followed by feature extraction and classification. In 2007, M. Dolejsi *et al.*[8] proposed an algorithm for segmentation of nodules in two separate ways, morphological closing and thresholding to find juxtapleural nodules and 3D blob detector with multiscale filtration to locate non-pleural nodule candidates. For classification, linear and multi-threshold classifiers were used. In 2007, Osman *et al.*[9] proposed a CAD system using template matching over the 3D volume to generate candidates. The false positive reduction was made using connected components and the sum of differences of densities in the surrounding pixels. In 2012, V. Sudha *et al.*[10] proposed a global thresholding algorithm following an iterative approach for lung volume extraction. The nodule segmentation stage was made by thresholding and morphological reconstruction. Another method, using template matching for nodule segmentation, was proposed by A.Tartar *et al.*[11] in 2013. The false positive reduction was made by decision trees. More algorithms using morphological operations for candidate extraction and different types of classifiers for false positive reduction have been proposed.[1213]

In the case of deep learning strategies, most of the research has focused on the classification of nodules starting from 2D or 3D nodule images using the LIDC-IDRI[3] dataset,[141516] the LUNA16 challenge dataset (which uses LIDC-IDRI), and the Multicentric Italian Lung Detection (MILD)[17] trial.[18] In these cases, the problem is addressed as a classification of nodules from given candidate centroids detected with previously published CAD systems.[19 20 21 22 23] The number of false positives to be classified is almost 25 times less than our extracted candidates but the highest sensitivity reached by these methods is around 87% (in the candidate generation stage) for all sized nodules. Since the nodule classification algorithms are evaluated over the total previously detected nodules and not over the total ground-truth nodules of each patient, the classification of nodules from previously detected algorithms is a problem with a lower difficulty degree.

3. PROPOSED METHOD

3.1 Lung volume filtering and masking

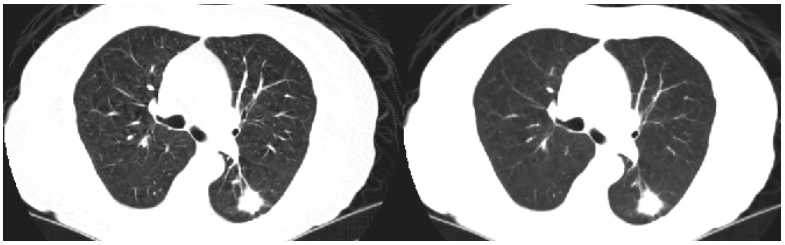

Figure 3. Volume filtering to reduce noise from the original patient's CT scan. **Left.** Original volume. **Right.** Filtered volume using median filter.

We generate candidates of each patient over the entire isotropic lung volume to benefit from the three-dimensional information provided by the CT scans. We transform the original CT volume to an isotropic volume in order to work with the same voxel size in all patient's CT scans. We filter the volume using a 3D median filter[24] for noise reduction. An example of a filtered volume is shown in Figure 3. After filtering, we extract the lung volume with a calculated mask to avoid unnecessary information which may lead to increased number of false positives. This mask is produced for each patient with a thresholding using a linear combination of the mean and standard deviation of each scan independently. Given that CT scans in the dataset are produced by different machines, a fixed threshold does not give good results. Following thresholding, we use morphological operations such as morphological closing to fill borders and holes and to remove small objects and structures connected to image border. A resulting mask example is shown in Figure 4b.

3.2 Candidate generation

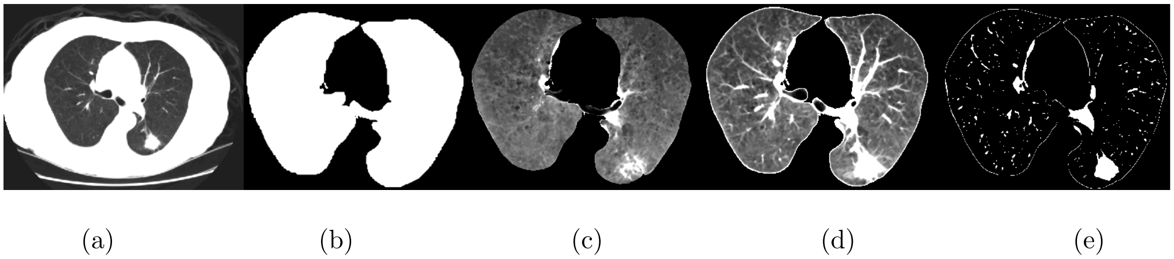

Figure 4. Masking and candidate extraction process. **(a)** Filtered volume with median filter. **(b)** Calculated lung mask with thresholding and morphological operations. **(c)** Lungs after erosion. **(d)** Lungs after opening by reconstruction. **(e)** Regional maxima calculation.

For candidate generation, we perform an opening by reconstruction over the extracted lung volume. We use this morphological operation given that the candidates are lighter regions in the scan. We need a marker volume created by eroding the 3D volume with an ellipsoid. The radius of the ellipsoid is 1 pixel and the height is the separation between two slices in each patient's volume. We carry out the morphological reconstruction using the marker described before and the filtered image as template. In addition, we calculate the regional maxima. Figure 4c to 4e shows the result after erosion, opening and regional maxima respectively. As it is shown in Figure

5, the objective of the candidate generation is to extract all light components (higher density tissue) inside the lungs.

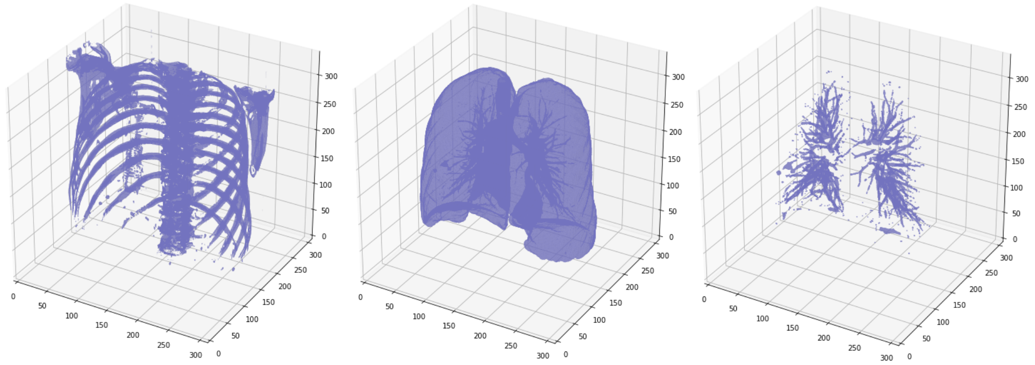

Figure 5. Three-dimensional view of different CT components. **Left.** Structures removed with mask. **Center.** Lungs after extraction with mask. **Right.** Extracted components.

3.3 Nodule classification

From the regional maxima, we compute the connected components per patient and their centroids. As shown in Figure 6, we perform a cleaning stage of negatives around the annotations with a predefined estimated radius for the training dataset (non-maximum suppression for validation and test datasets). We do the cleaning only for training computed centroids in order to avoid using candidates that look like annotations but with a negative label in the neural network training.

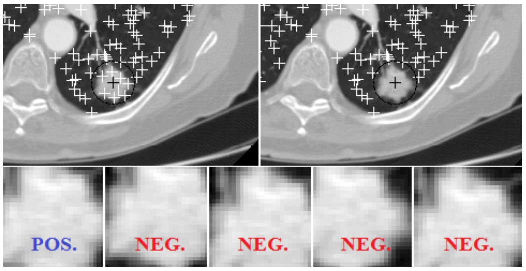

Figure 6. Cleaning of negatives around the annotations. **Top-left**. Computed centroids without cleaning. **Top-right**. Computed centroids with cleaning. **Bottom**. Extracted candidates and corresponding label without cleaning.

We design and train a three-dimensional convolutional neural network (3D CNN) for false positive reduction with 3D candidates (volumes centered at the calculated centroid) as input. In contrast of 2D CNN, when we use 3D convolutions we analyze one additional spatial dimension which is important to differentiate nodules from other structures such as vessels that may look similar in one slice independently.

We define a modular network for the systematized exploration of CNN architectures. It consists of groups of convolutional layers with filters of a fixed size 3 by 3, batch normalization, and ReLu activations. The filters are tested with a fixed number in all layers, or duplicating them after each max. pooling. In the experiments, we change the number of convolutional layers before each pooling layer, the number of filters, and the value of hyperparameters such as batch size and learning rate. Also, the number of max. pooling layers is changed depending on the input size of the network, resulting in feature maps in the last convolutional layer with size from 2x2 to 12x12.

4. EXPERIMENTS

4.1 Dataset

The dataset is produced by the Lung Image Database Consortium (LIDC) and the Image Database Resource Initiative (IDRI)[3] with a total of 1.006 patients. It is publicly available in DICOM format and the radiologists' annotations in XML markup. The annotations are made by 4 radiologists in two stages; a blind stage and a second unblinded stage where each radiologist is presented with the marks placed by all radiologists in the blind stage. For this project we consider lesions labeled as nodules for at least one specialist and included after the unblinded second stage.

Table 1 shows the consensus in lung-nodule detection by the four radiologists. As we can see, only 51,4% of the total included nodules after the unblinded second stage are detected by the 4 specialists, and only 27.8% of the total nodules from the blind initial stage. The consensus of 51.4%, which we will use as human performance for this task, shows the difficulty of detecting lung nodules.

Table 1. Annotations statistics from the LIDC-IDRI dataset

Patients	1006		
Total nodules labeled	11.608	100%	
Total nodules included	6.287	54.2%	100%
Nodules included by 4 annotators	3.233	27.8%	**51.4%**

We divide the dataset randomly into 3 sets; 25% of patients for training, 25% for validation, and the remaining 50% for testing.

4.2 Validation experiments

Candidate generation. For candidate generation, we test different configurations of thresholding equations, several values for the erosion ellipsoid's radius and height, and different input connectivities. The best recall we obtained for this stage is 99,6% with 3.154 included nodules (of 3.167) from a total of 25.221.581 generated candidates from the training/validation set. That gives a total of 25.218.427 false positives.

The total amount of candidates for the training/validation set is around 25 million with approximately 3.150 positive nodules (included in the annotations), which is extremely unbalanced. As a consequence, we perform a data augmentation with image translations and horizontal reflections for each candidate. From the 3.150 positive nodules, we augment (by a factor of x216) to around 700.000 to have a representative number of positive nodules for the training of the CNN. We select randomly the same number of negatives (non-nodules) after augmentation to balance the training dataset. Therefore, our training/validation set is composed of around 1.4 million candidates.

False positive reduction. Due to the variability of intensities in a CT scan and the gray-scale nature of the images, we consider as a baseline histogram of oriented gradients (HOG) for feature extraction of each candidate and train a support vector machine (SVM) for false positive reduction because of its proven good performance as shape feature discriminator.[25] Although precision improves, the number of false positives remains high. Training a convolutional neural network, the precision increases considerably from the candidate extraction.

We test 2D and 3D convolutions using the MexConv3D[26] library. For the 2D convolutions, we used 32x32x3 candidates as input for the network, using the axial, sagittal and coronal planes centered on the calculated (Section 3.2) centroid, for the first case (See Figure 7a). We take this first approach for its simplicity and low GPU memory usage. For the second case, we use 2D convolutions on 32x32x9 candidates, using the 9 consecutive z-planes from the centroid (See Figure 7b). In this case, we want to include more spatial information of each candidate and increase the precision. The best results we obtain are using 3D convolutions with filters of size 3x3x3 and input volume size of 24x24x24. As shown in Figure 9, we increase precision for all recall values with the 3D CNN approach.

Table 2 shows results with different input size for the 3D CNN approach. The three-dimensional convolutional neural network is trained with different input size candidates. The first approach is using candidates of size 32x32x9 that gives best results with bi-dimensional convolutional neural networks. The AP we obtain with this

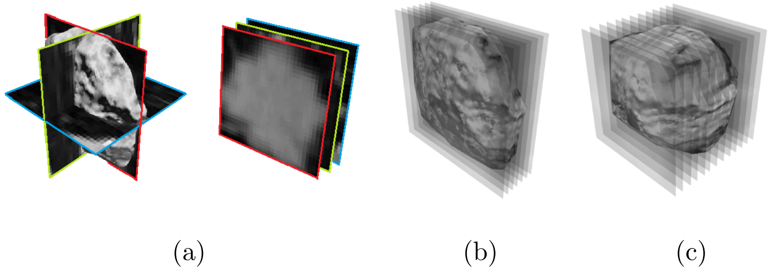

Figure 7. Candidate modalities. **(a)**. 32x32x3 candidate with axial, sagittal and coronal planes. **(b)**. 32x32x9 candidate using 9 consecutive z-planes. **(c)**. 24x24x24 candidate (Best result).

candidate size is less than using 2D convolutions (35.6% with 3D convolutions and 36.7% with 2D convolutions). Then, we use smaller candidate size (16x16x16 instead of 32x32x9), but with more z-planes (16 planes instead of 9). The result is not better than with 32x32x9 candidates but it is very similar even with less than half number of voxels. Finally, we increase the candidate size to 24x24x24 with which we obtain the best results.

Table 2. Results using different candidate size as input for 3D CNNs

Input Size	**# Voxels**	**AP (%)**
32 x 32 x 9	9.216	35.6
16 x 16 x 16 (Isotropic)	4.096	34.7
24 x 24 x 24 (Isotropic)	13.824	**44.8**

Table 3 presents experiments changing the number of convolutional layers inside the 3D CNN.

Table 3. Results with different number and distribution of convolutional layers

Conv. layer array*	**# Conv. layers**	**AP (%)**
2 > 2 > 2 -fc -sm	6	41.0
2 > 2 > 2 > 2 -fc -sm	8	41.2
3 > 3 > 3 -fc -sm	9	42.9
3 > 3 > 3 > 3 -fc -sm	12	37.0
4 > 4 > 4 -fc -sm	12	42.6
3 > 4 > 5 -fc -sm	12	**44.8**
4 > 5 > 6 -fc -sm	15	34.8

* > : max. pooling layer
-fc : fully connected layer
-sm : softmax

As we can see, the depth of the network is not the only factor increasing the performance of the system. For the particular case of 15 layers shown in Table 3, the decrease in average precision may be caused by over-fitting to the training data, which causes a decrease in the generalization of the network.

Regarding the batch size, the trend is that the performance is better when it is smaller, the final batch size chosen is of 16 images. As for the number of filters, we obtain the best results when the number (128 filters) is held constant in all layers. As for batch normalization, the performance of the network increases considerably after using it.

We obtain our best results by employing a neural network consisting of twelve 3D convolutional layers and one fully connected layer before the softmax that produces a probability of nodule/non-nodule. We also use max pooling after the 3rd and 7th layers. We use batch normalization for all convolutional layers, and the activation function for each one is a rectified linear unit (ReLu). ReLu is used to create non-linearities that reduce over-fitting and regularize training. The network architecture is shown in Figure 8.

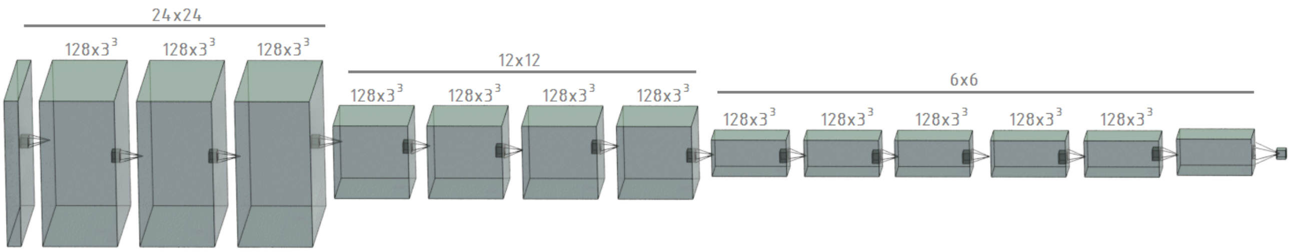

Figure 8. Neural network architecture of twelve 3D convolutional layers with best results from our modular design of 3x3x3 filters.

We train the network from scratch using stochastic gradient descent and back-propagation with a fixed learning rate of 0,0001. We perform the training during 15 epochs. The evaluation is performed on the test set with an average precision (AP) of 44.8%.

As shown in Table 4, the average precision obtained with deep learning methods is increased to a greater extent than using HOG and SVM. In the other hand, using three-dimensional convolutional neural networks gives the best results.

Figure 9 shows precision-recall curves of the results evaluated in the test set of the different methods used. We can see that the precision is greatly increased for all recall values using convolutional neural networks.

Table 4. Average precision obtained with different false positive reduction methods

Method	**AP (%)**
No FP reduction method	0.0062
HOG + SVM	0.021
CNN 2D	8.9
CNN 2.5D	36.7
CNN 3D	**44.8**

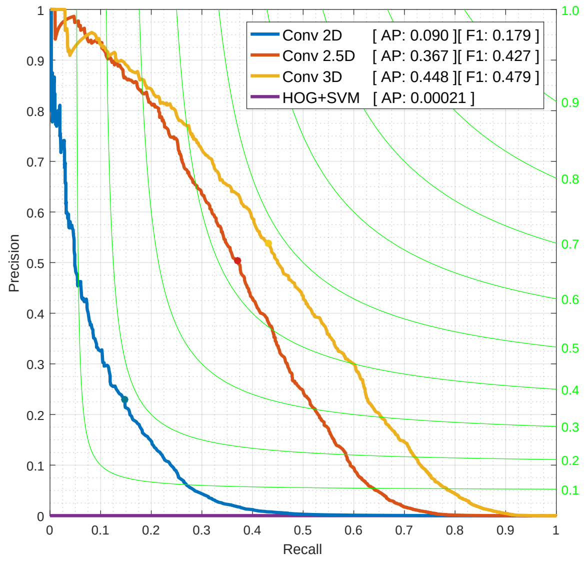

Figure 9. Comparison between false positive reduction methods. HOG+SVM and best networks using convolutions in 2D, 2.5D (2D convolutions over 3D candidates) and 3D.

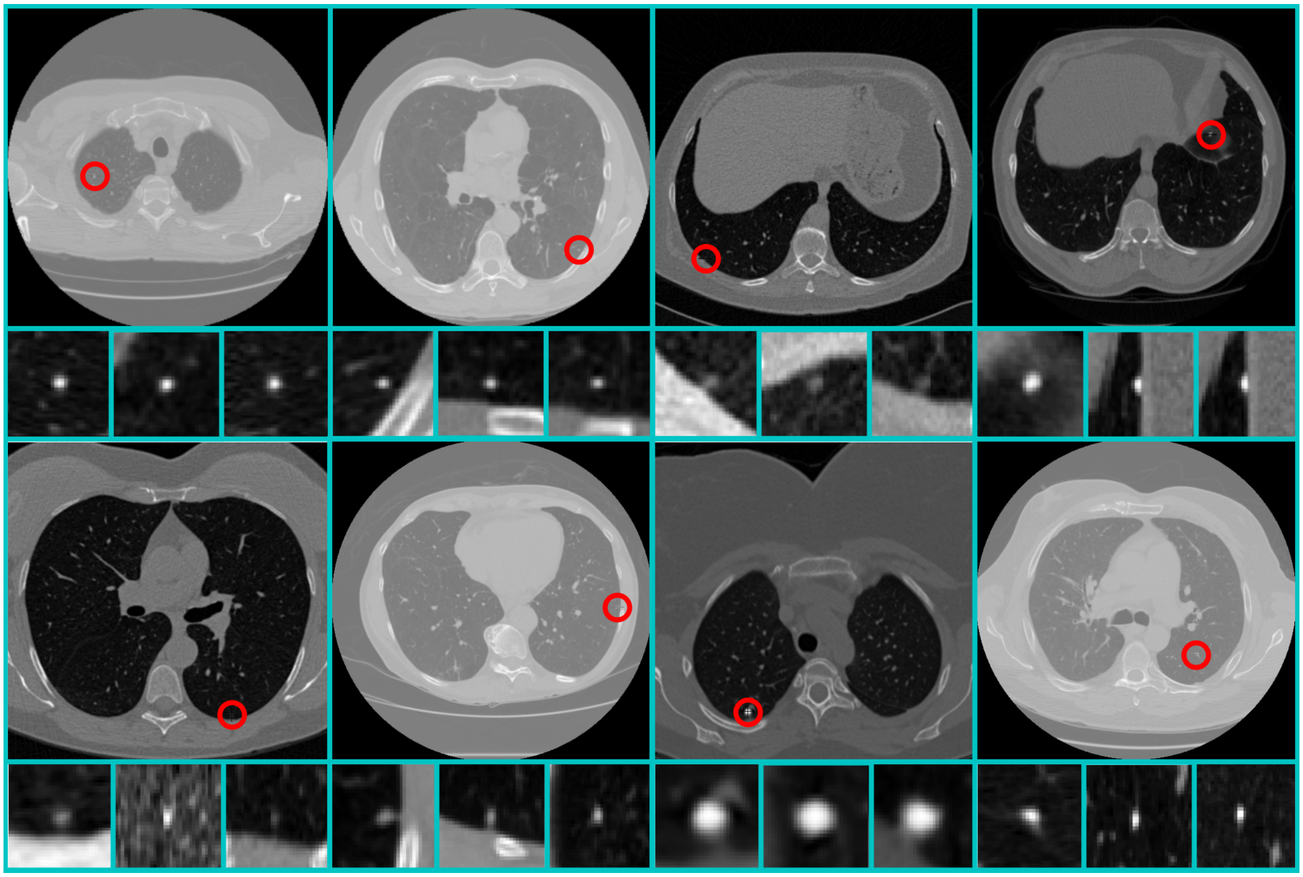

Figure 10. Qualitative results of high scored nodule detections.

5. CONCLUSIONS

Although the problem of nodule detection is extremely unbalanced with high intra-class variance, our approach is able to detect and classify lung nodules effectively. We design a candidate proposal method with almost perfect recall. In addition, we train a three-dimensional convolutional neural network that successfully classifies nodules from non-nodules and increases the precision by a factor of 7.000 achieving a close-to-human performance in this challenging task.

The strongest limitation that we have identified -the one that most profoundly impacts our results- is the lack of consistency in the annotations among the radiologists. In Figure 10 (left), we show some examples of nodules marked as positive in the annotations (green), and small round or oval-shaped growth that were not annotated by any radiologist (red). The lack of consistency in the annotations limits our ability to properly quantify the average precision of our method. However, as shown in figure 10, the algorithm is capable of detecting small round or oval-shaped growth with high density in the lungs that are clearly not vessels and were not originally labeled as nodules.

Nodules with atypical morphology are also problematic. Although they are usually annotated in the database, they differ greatly from most other nodules, thus are subrepresented. We show an example of atypical lesions in figure 10 (right). One possible strategy to address this problem is to identify these nodules and augment this data, as to reduce underrepresentation in the training set.

6. ACKNOWLEDGEMENTS

We gratefully acknowledge the support from NVIDIA Corporation for providing us the GPUs used in this research.

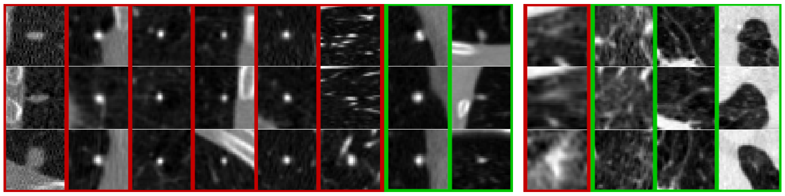

(a)

(b)

Figure 11. **(a) Annotation inconsistency.** (Red) Negative nodules (not annotated nodules) with high score. (Green), nodule labeled in the annotations as positive with high score. **(b) Atypical cases.** (Red), negative nodule with high score. (Green), nodules labeled in the annotations as positives.

REFERENCES

[1] "World Health Organization. Media Centre, Cancer." urlhttp://www.who.int/mediacentre/factsheets/fs297/en/ (2017).

[2] "American Cancer Society. Cancer Facts and Figures 2015," (2015). Atlanta: American Cancer Society.

[3] S. G. Armato III et al., "The Lung Image Database Consortium LIDC and Image Database Resource Initiative (IDRI): A Completed Reference Database of Lung Nodules on CT Scans," *Medical Physics* **38**(2), 915–931 (2011).

[4] Q. Li, "Recent progress in computer-aided diagnosis of lung nodules on thin-section CT.," *Comput Med Imaging Graph* **31**, 248–257 (June 2007).

[5] S.L.A. Lee and A.Z. Kouzani and E.J. Hu, "Automated detection of ling nodules in computed tomography images: a review.," *Mach Vis Appl* **23**, 151–163 (2012).

[6] B. V. Ginneken, et al., "Comparing and combining algorithms for computer-aided detection of pulmonary nodules in computed tomography scans: The ANODE09 study," *Medical Image Analysis* **14**, 707–722 (2010).

[7] A. Esteva, et al., "Dermatologist-level classification of skin cancer with deep neural networks," *Nature* **542**, 115–126 (2017).

[8] M. Dolejsi and J. Kybic, "Automatic two-step detection of pulmonary nodules," *Proceedings of SPIE* **6514**, 3j–1–3j–12 (2007).

[9] S. O. O. Osman and O. N. Ucan, "Lung nodule diagnosis using 3d template matching," *Comput. Biol. Med.* **37**, 1167–1172 (2007).

[10] V. Sudha and P. Jayashree, "Lung nodule detection in CT images using thresholding and morphological operations," *International Journal on Emerging Science and Engineering (IJESE)* **1**, 17–21 (Dec. 2012).

[11] A.Tartar and A. Akan, "A new method for pulmonary nodule detection using decision trees," *35th Annual International Conference of the IEEE EMBS* (2013).

[12] C. Jacobs, et al., "Automatic detection of subsolid pulmonary nodules in thoracic computed tomography images," *Medical Image Analysis* **18**, 374–384 (2014).

[13] A. Oseas, et al., "Automatic detection of solitary lung nodules using quality threshold clustering, genetic algorithm and diversity index," *Artifitial Intelligence in Medicine* **60**, 165–177 (2014).

[14] S. Hussein, et al., "Risk Stratification of Lung Nodules Using 3D CNN-Based Multi-task Learning," *IPMI* (2017).

[15] K. Song, et al., "Using Deep Learning for Classification of Lung Nodules on Computed Tomography Images," (2015).

[16] W. Sun, et al., "computer aided Lung Cancer Diagnosis with Deep Learning Algorithms," *Research gate* (2016).

[17] U. Pastorino, et al., "Annual or biennal CT screening versus observation in heavy smokers: 5-year results of the MILD trial," *Euroopean Journal of Cancer Prevention* (2012).

[18] F. Ciompi, et al., "Towards automatic pulmonary nodule management in lung cancer screening with deep learning," (2017).

[19] K. Murphy, et al., “A large scale evaluation of automatic pulmonary nodule detection in chest CT using local image features and k-nearest-neighbour classification,” *Medical Image Analysis* **13**, 757–770 (2009).

[20] C. Jacobs, et al., “Automatic detection of subsolid pulmonary nodules in thoracic computed tomography images,” *Medical Image Analysis* **18**, 374–384 (2014).

[21] A. Setio, et al., “Automatic detection of large pulmonary solid nodules in thoracic CT images,” *Medical Physics* **42**, 5642–5653 (2015).

[22] M. Tan, et al., “A novel computer-aided lung nodule detection system for CT images,” *Medical Physics* **38**, 5630–5645 (2011).

[23] E. Torres, et al., “Large scale validation of the M5L lung CAD on heterogeneous CT datasets,” *Medical Physics* **42**, 1477–1489 (2015).

[24] D. Garcia, “”Medfilt3.m”,” (2007).

[25] N. Dalal, et al., “Histograms of Oriented Gradients for Human Detection,” *CVPR* (2005).

[26] P. Sun, “MexConv3D.” urlhttps://github.com/pengsun/MexConv3D (2015).